

Equiangular Fan-Beam CT Reconstruction for a Non-Circular Scanning Locus

Katherine Redford
Ge Wang, Ph.D.
Michael W. Vannier, M.D.

January 19, 2000

Department of Radiology
University of Iowa Hospitals and Clinics
200 Hawkins Drive
Iowa City, Iowa 52242, USA
Phone: (319) 341-8620
Fax: (319) 356-2220
E-mail: kredford@icaen.uiowa.edu
ge-wang@uiowa.edu
michael-vannier@uiowa.edu

Abstract

A derivative-free, two-dimensional equiangular fan-beam reconstruction formula for a non-circular scanning locus is derived under three practical conditions. The reconstruction formula for a non-circular scanning locus contains the same terms as the traditional formula, except that the constant source-to-origin distance is replaced by the source-to-origin distance as a function of the rotation angle. The correctness of this formula is tested in numerical simulation. The potential applications of the formula include fourth generation CT, electron beam CT, SPECT, and X-ray microtomography.

Subject Terms: medical imaging, X-rays, image reconstruction, image quality, imaging system, microscopy

Introduction

Computerized tomography (CT) is based on reconstruction of an image from line integrals. CT has found many applications in diverse fields. In medical applications, line integrals, also referred to as projections, of an object are measured using X-rays. The X-rays travel through the object along straight lines, are attenuated by the object, and detected outside the object. Parallel-beam scanning is achieved through translation and rotation of an assembly of an X-ray source and a single detector so that all line integrals through an object are collected. Fan-beam scanning utilizes a single X-ray source and multiple detectors. The X-ray source and detectors define a fan of X-rays that covers the entire cross-section being imaged. Similar to the parallel-beam case, fan-beam projection data are collected from various angles [4].

Some scanners employ a single detector array which rotates with the source, while others utilize stationary detectors with a rotating X-ray source. Detectors may be arranged in an arc with equiangular spacing, or along a straight line with equal spatial distance. Today's CT scanners use both equispacial and equiangular formats, but the equiangular geometry is used more often for medical X-ray CT because equiangular arrangement of detectors usually leads to a more compact design and a smaller source-to-detector distance. Equiangular fan-beam scanning based spiral/helical CT has become the standard in medical X-ray CT [4].

An equispacial fan-beam reconstruction formula with a non-circular scanning locus has already been derived under three practical conditions. This simple formula contains no derivative term of the scanning locus with respect to the rotation angle, and is advantageous for several imaging modalities [5]. In this communication, we derive a counterpart formula in the equiangular geometry under the same conditions, test the correctness of the formula in numerical simulation, and discuss its potential applications.

Derivation

The reconstruction formula for equiangular fan-beam projection data with a circular scanning locus is:

$$f(r, \phi) = \frac{1}{2} \int_0^{2\pi} \int_{-\gamma_m}^{\gamma_m} R_{\beta(\gamma)} h [r \cos(\beta + \gamma - \phi) - D \sin \gamma] D \cos \gamma d\gamma d\beta \quad (1)$$

where D is a constant source-to-origin distance [3]. If the scanning locus is not circular, however, D will vary with the rotation angle β by the function $D(\beta)$. Intuitively, we predict that the reconstruction formula for the non-circular scanning case will contain the same terms as the circular case, replacing D by $D(\beta)$:

$$f(r, \phi) = \frac{1}{2} \int_0^{2\pi} \int_{-\gamma_m}^{\gamma_m} R_{\beta(\gamma)} h [r \cos(\beta + \gamma - \phi) - D(\beta) \sin \gamma] \cdot D(\beta) \cos \gamma d\gamma d\beta \quad (2)$$

The detailed mathematical proof of this formula follows.

The formula developed for non-circular, equiangular ray fan beam data is exact under the following conditions:

1. $D(\beta) = D(\beta + \pi)$
2. $D'(\beta)$ exists almost everywhere
3. $D^2(\beta) > D'(\beta)_{\gamma_m}$, where γ_m is the minimum value such that $R_{\beta(\gamma)} = 0$, if $|\gamma| > \gamma$.

These conditions are generally satisfied. In particular, the third condition holds when the source-to-origin distance $D(\beta)$ is large, and $D'(\beta)$ is small.

We begin with the parallel projection $P_{\theta}(t)$ representation of $f(r, \phi)$ [3]:

$$f(r, \phi) = \frac{1}{2} \int_0^{2\pi} \int_{-t_m}^{t_m} P_{\theta}(t) h [r \cos(\theta - \phi) - t] dt d\theta \quad (3)$$

Where, in the fan beam case,

$$\theta = \beta + \gamma \quad (4)$$

$$t = D(\beta) \sin \gamma \quad (5)$$

β = the angle subtended by the source S and the reference axis

γ = the location of a specific ray in the fan

$D(\beta)$ = the distance between the source S and the origin O

x = $r \cos \phi$

y = $r \sin \phi$

$P_{\theta}(t)$ = parallel projection data

$$\begin{aligned}
t_m &= t \text{ for which } P_\theta(t) = 0 \text{ with } |t| > t_m \\
h(\gamma) &= \int_{-\infty}^{\infty} |\omega| e^{j2\pi\omega\gamma} d\omega
\end{aligned}$$

These parameters are shown in the fan-beam geometry in Fig. 1.

Solving (4) for β , we obtain:

$$\beta = \theta - \gamma \quad (6)$$

Solving (5) for γ , we obtain:

$$\gamma = \sin^{-1} \left(\frac{t}{D(\beta)} \right) \quad (7)$$

Differentiating (4) and (5), we find:

$$\begin{aligned}
\frac{\delta t}{\delta \gamma} &= D(\beta) \cos \gamma \\
\frac{\delta \theta}{\delta \gamma} &= 1 \\
\frac{\delta t}{\delta \beta} &= D'(\beta) \sin \gamma \\
\frac{\delta \theta}{\delta \beta} &= 1
\end{aligned}$$

Using the Jacobian and the third condition:

$$dt d\theta = [D(\beta) \cos \gamma - D'(\beta) \sin \gamma] d\gamma d\beta \quad (8)$$

Performing a change of variables with (6), (7), and (8):

$$\begin{aligned}
f(r, \phi) &= \frac{1}{2} \int_0^{2\pi} \int_{-\gamma_m}^{\gamma_m} P_{\beta+\gamma} [D(\beta) \sin \gamma] h [r \cos(\beta + \gamma - \phi) - D(\beta) \sin \gamma] \\
&\quad \cdot [D(\beta) \cos \gamma - D'(\beta) \sin \gamma] d\gamma d\beta
\end{aligned}$$

The integral may be expanded and separated to give one integral with the term $D(\beta) \cos \gamma$ and one integral with the term $D'(\beta) \sin \gamma$. Splitting the latter integral into two parts, I_1 and I_2 :

$$\begin{aligned}
I_1 + I_2 &= \int_0^\pi \int_{-\gamma_m}^{\gamma_m} P_{\beta+\gamma} [D(\beta) \sin \gamma] h [r \cos(\beta + \gamma - \phi) - D(\beta) \sin \gamma] D'(\beta) \sin \gamma d\gamma d\beta \\
&\quad + \int_\pi^{2\pi} \int_{-\gamma_m}^{\gamma_m} P_{\beta+\gamma} [D(\beta) \sin \gamma] h [r \cos(\beta + \gamma - \phi) - D(\beta) \sin \gamma] D'(\beta) \sin \gamma d\gamma d\beta
\end{aligned}$$

Since $P_{\theta+\pi}(-t) = P_{\theta}(t)$, $D(\beta+\pi) = D(\beta)$, $D'(\beta+\pi) = D'(\beta)$ and $h(-p) = h(p)$,

$$\begin{aligned} I_2 &= \int_0^{\pi} \int_{-\gamma_m}^{\gamma_m} P_{\beta+\gamma} [-D(\beta) \sin \gamma] h [-r \cos(\beta + \gamma - \phi) - D(\beta) \sin \gamma] [-D'(\beta) \sin \gamma] d\gamma d\beta \\ &= - \int_0^{\pi} \int_{-\gamma_m}^{\gamma_m} P_{\beta+\gamma} [D(\beta) \sin \gamma] h [r \cos(\beta + \gamma - \phi) - D(\beta) \sin \gamma] D'(\beta) \sin \gamma d\gamma d\beta \\ &= -I_1 \end{aligned}$$

Therefore, $I_1 + I_2 = I_1 - I_1 = 0$. With this property, the integral with the term $D'(\beta) \sin \gamma$ drops out and $f(r, \phi)$ becomes:

$$f(r, \phi) = \frac{1}{2} \int_0^{2\pi} \int_{-\gamma_m}^{\gamma_m} P_{\beta+\gamma} [D(\beta) \sin \gamma] h [r \cos(\beta + \gamma - \phi) - D(\beta) \sin \gamma] D(\beta) \cos \gamma d\gamma d\beta$$

But $P_{\beta+\gamma} [D(\beta) \sin \gamma]$ is just $R_{\beta(\gamma)}$ in the fan projection, so

$$f(r, \phi) = \frac{1}{2} \int_0^{2\pi} \int_{-\gamma_m}^{\gamma_m} R_{\beta(\gamma)} h [r \cos(\beta + \gamma - \phi) - D(\beta) \sin \gamma] D(\beta) \cos \gamma d\gamma d\beta$$

This formula corresponds exactly with the predicted formula (2); that is, the same terms appear in the non-circular scanning case as in the circular case. In terms of x and y , the formula for the non-circular scanning case is as follows:

$$f(x, y) = \frac{1}{2} \int_0^{2\pi} \int_{-\infty}^{\infty} R_{\beta(\gamma)} h [x \cos(\beta + \gamma) + y \sin(\beta + \gamma) - D(\beta) \sin \gamma] D(\beta) \cos \gamma d\gamma d\beta$$

Computer Simulation

Computer simulation was used to test the reconstruction algorithm. A computer program written in the Interactive Data Language (IDL) was used to implement the simulation. Tests were performed using a three-dimensional Shepp-Logan phantom with x and y dimensions 112 by 112. Because the attenuation constants in the Shepp-Logan phantom were known (Table 1), the theoretical projection values were easily calculated. Using these projection values, the phantom was reconstructed in the circular and elliptical scanning cases using the IDL program. In the elliptical case, the ratio of the long-axis to the short-axis was 1.2. Linear interpolation was used to find the projection value corresponding to each detector for a given rotation angle. Filtered backprojection was performed using 100 projections, 128 detectors, and full-scan scanning. A point source and point detectors were assumed.

No.	x_0	y_0	z_0	a	b	c	α	τ
1	0.00	0.000	0.000	0.6900	0.920	0.900	0	2.00
2	0.00	0.000	0.000	0.6624	0.874	0.880	0	-0.98
3	-0.22	0.000	-0.250	0.4100	0.160	0.210	108	-0.02
4	0.22	0.000	-0.250	0.3100	0.110	0.220	72	-0.02
5	0.00	0.350	-0.250	0.2100	0.250	0.500	0	0.02
6	0.00	0.100	-0.250	0.0460	0.046	0.046	0	0.02
7	-0.08	-0.650	-0.250	0.0460	0.023	0.020	0	0.01
8	0.06	-0.650	-0.250	0.0460	0.023	0.020	90	0.01
9	0.06	-0.105	0.625	0.0560	0.040	0.100	90	0.02
10	0.00	0.100	0.625	0.0560	0.056	0.100	0	-0.02

Table 1: Parameters of Shepp and Logan’s three-dimensional head phantom used in the simulation.

Results

Comparison of the ideal images at two transaxial levels with the corresponding reconstructed images are shown in Figure 2. Profiles through a representative line in the field of view are superimposed in Figure 3. While some differences in aliasing effects were noticeable in un-windowed images, Figures 2 and 3 show the close similarity of the reconstruction results. Biasing occurred while using the general reconstruction formula due to the asymmetric nature of the elliptical scanning locus. Increasing the number of detectors used in the simulation reduced these effects. In all cases, the computational complexity of both algorithms was comparable.

Discussion

Our non-circular equiangular fan-beam formula may find an application in fourth-generation CT scanners. These scanners feature a stationary detector ring and a rotating x-ray source, as shown in Fig. 4. For each position of the X-ray source, a ray strikes every detector [4]. In this way, the shape of the detector array determines the scanning locus. The generalized equiangular formula presented here would allow reconstruction of an image collected with an elliptical or otherwise non-circular detector array. Use of a non-circular detector array could bring the detector closer to the patient and X-ray source. Since the signal intensity is inversely proportional to the source-to-detector distance squared, the signal intensity would increase, thereby increasing the signal-to-noise ratio.

Our non-circular equiangular formula may also be applied with electron-

beam CT scanners. An electron-beam scanner includes a stationary arc of detectors and a sweeping X-ray source, as shown in Fig. 5. Considering each stationary detector as the apex of a fan, the detector shape determines the scanning locus of the geometry [1,4]. Changing the geometry of the detector array from circular to elliptical shape allows the detector array to intercept the X-ray photons earlier, which can be translated into a better signal-to-noise ratio as described above.

Imaging using a single photon emission computed tomography (SPECT) system with a rotating scintillation camera introduces another non-circular scanning locus. In this modality, the camera follows the contour of the body, rotating in a non-circular orbit to achieve the best magnification of the section of interest [2]. The derivative-free fan-beam formula would provide a means of reconstructing images for such a SPECT system.

In X-ray microtomography, noncircular scanning loci are useful, including polygonal and helix-like loci [6]. The non-circular equiangular fan-beam formula provides opportunities for optimizing the system configuration and the image quality. For example, the current reconstruction formula requires mapping of the data onto the virtual flat array when the abutted detector array is polygonal in shape. If projection data were instead sorted into equiangular format, our formula could be used to reconstruct the image without interpolation blurring.

Conclusion

We have derived and tested the derivative-free equiangular fan-beam reconstruction formula for non-circular scanning loci. The new formula is the same as the conventional equiangular fan-beam formula, except that the constant source-to-origin distance is made a function with respect to the X-ray source rotation angle. This formula may be applied to electron-beam CT, fourth-generation CT, single photon emission CT, and X-ray microtomography for more compact system design and better image quality.

Acknowledgements

This work was supported in part by the grants from the National Institutes of Health (NIDDK R29 DK50184 and NINDS R01 NS35368).

References

1. D.P. Boyd and M.J. Lipton, "Cardiac computed tomography," *Proc. IEEE* 198-307 (1983).

2. G.T. Gullberg and G.L. Zeng, "A Cone-Beam Filtered Backprojection Reconstruction Algorithm for Cardiac Single Photon Emission Computed Tomography." *IEEE Trans. on Medical Imaging* 11(1), 91-101 (1992).
3. A.C. Kak and M. Slaney, *Principles of Computerized Tomographic Imaging*, IEEE Press, New York, NY (1987).
4. E. Seeram, *Computed Tomography: Physical Principles, Clinical Applications and Quality Control*, W.B. Saunders Company, Philadelphia, PA (1994).
5. G. Wang, T.H. Lin, and P.C. Cheng, "A derivative-free noncircular fan-beam reconstruction formula," *IEEE Trans. on Image Processing* 2(4), 543-547 (1993).
6. G. Wang, T.H. Lin, P.C. Cheng, and D.M. Shinozaki, "A General Cone-Beam Reconstruction Algorithm," *IEEE Trans. on Medical Imaging* 12(3), 486-495 (1993).

Figure and Table Captions

Figure 1. Equiangular fan beam geometry. Fan beam projections are sorted according to rotation angle β and sampling angle α .

Figure 2. Comparison between the ideal images and reconstructions with circular and elliptical scanning. (a) Ideal image, (b) circular and (c) elliptical scanning reconstructions for the slice at $z=-0.25$ of the three-dimensional Shepp-Logan phantom; (d) ideal image, (e) circular and (f) elliptical scanning reconstruction for the slice at $z=0.625$ of the Shepp-Logan phantom.

Figure 3. Plots of an ideal profile, corresponding profiles reconstructed at $y=0.22$, $z=-0.25$ of the three-dimensional Shepp-Logan phantom with circular and elliptical scanning.

Figure 4. Fourth generation CT scanner geometry. The non-circular scanning locus allows shorter X-ray source-to-detector distances, thereby increasing the signal to noise ratio.

Figure 5. Electron beam CT scanner geometry. The non-circular scanning locus allows shorter X-ray source-to-detector distances, thereby increasing the

signal to noise ratio.

Table 1. Parameters of Shepp and Logan's three-dimensional head phantom used in the simulation.

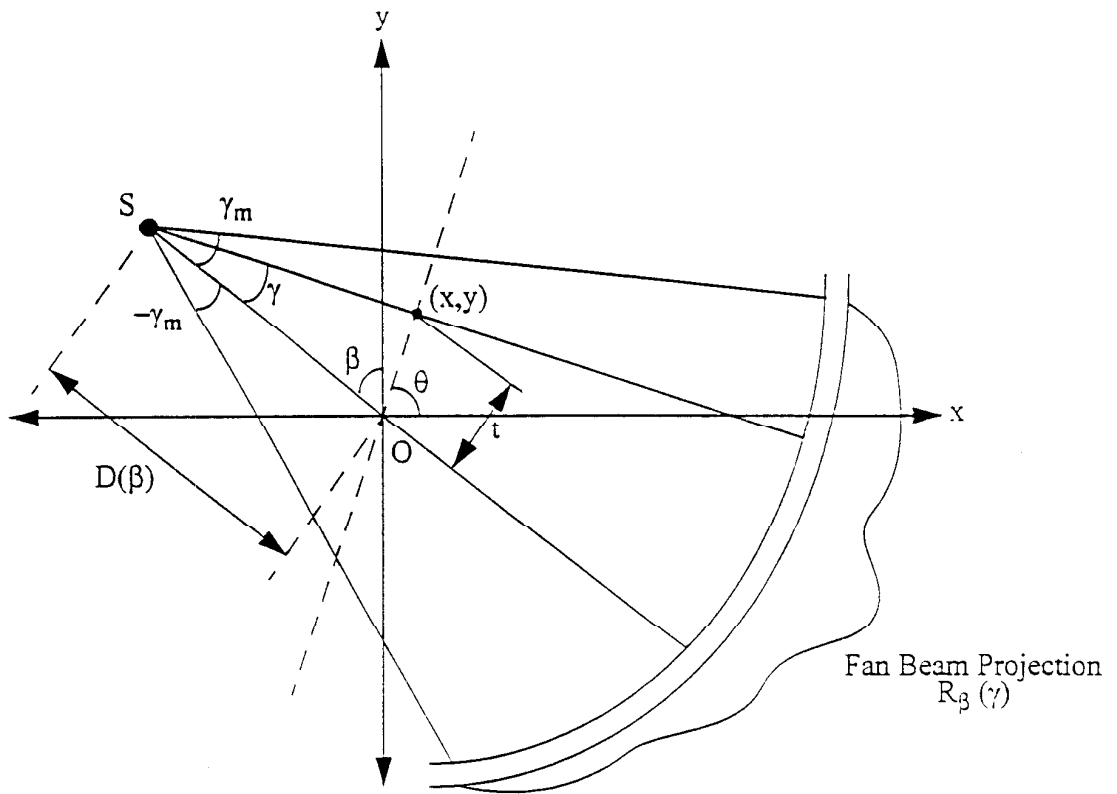


Figure 1. Equiangular fan beam geometry. Fan beam projections are sorted according to rotation angle β and sampling angle α .

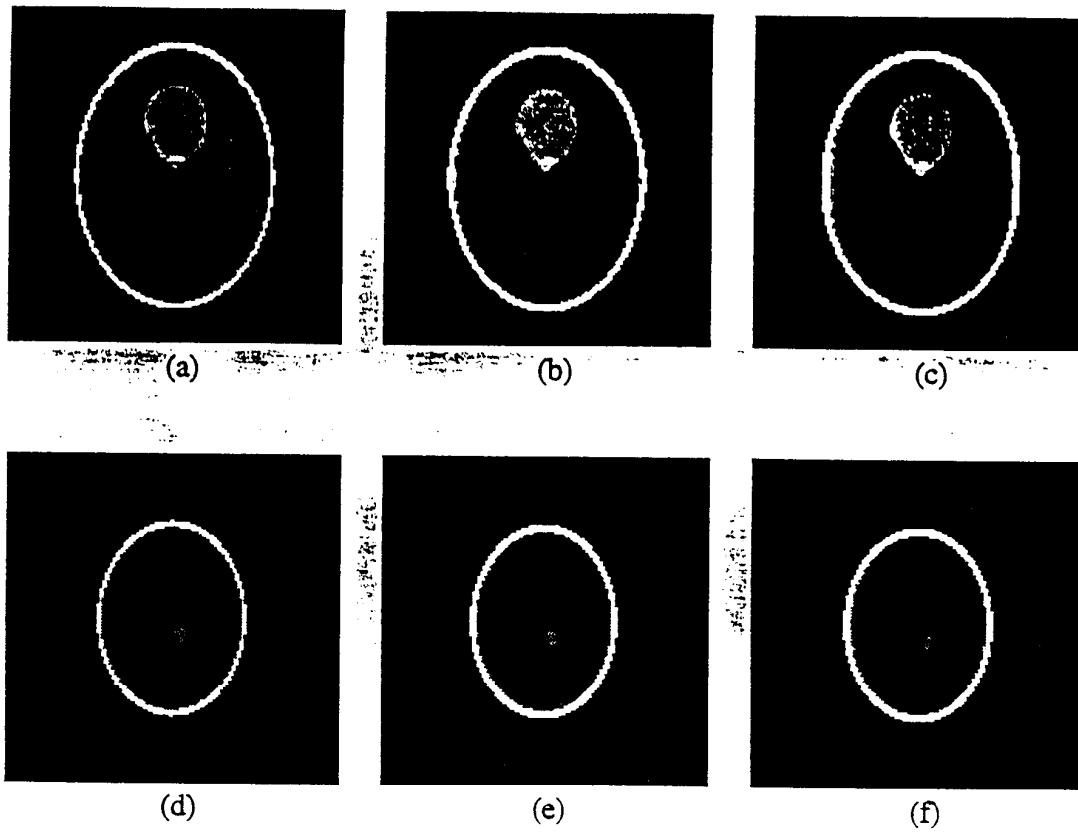


Figure 2. Comparison between the ideal images and reconstructions with circular and elliptical scanning. (a) Ideal image, (b) circular and (c) elliptical scanning reconstructions for the slice at $z = -0.25$ of the three-dimensional Shepp-Logan phantom; (d) ideal image, (e) circular and (f) elliptical scanning reconstruction for the slice at $z = 0.625$ of the Shepp-Logan phantom.

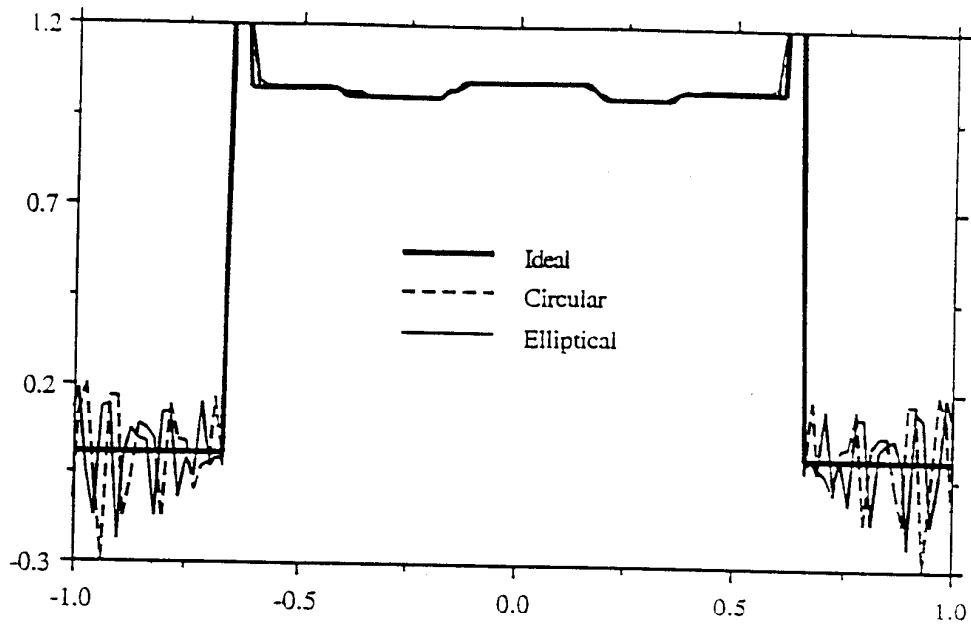


Figure 3. Plots of an ideal profile, corresponding profiles reconstructed at $y=0.22$, $z=-0.25$ of the three-dimensional Shepp-Logan phantom with circular and elliptical scanning.

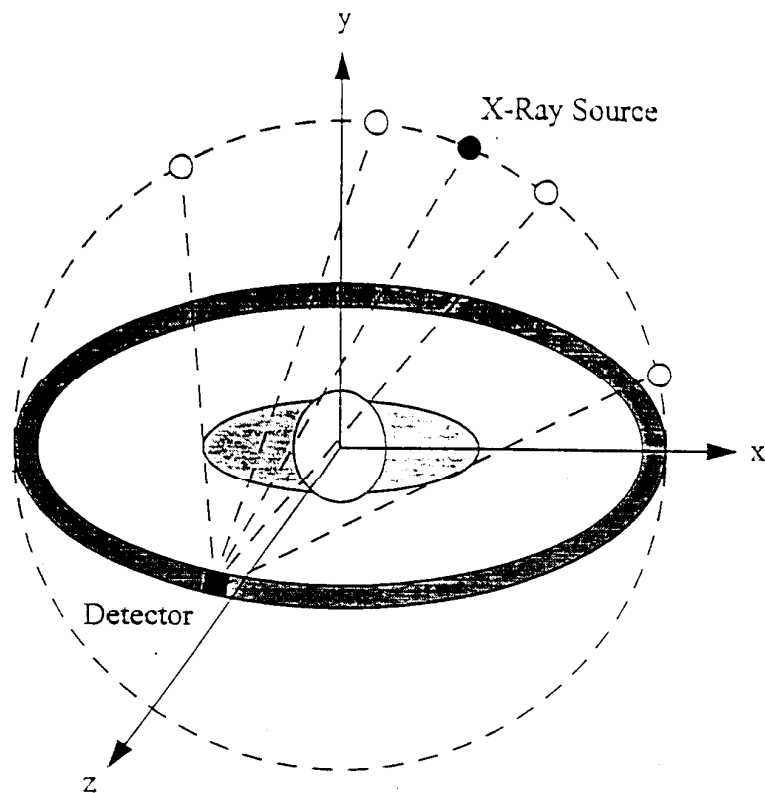


Figure 4. Fourth generation CT scanner geometry. The non-circular scanning locus allows shorter x-ray source-to-detector distances, thereby increasing the signal to noise ratio.

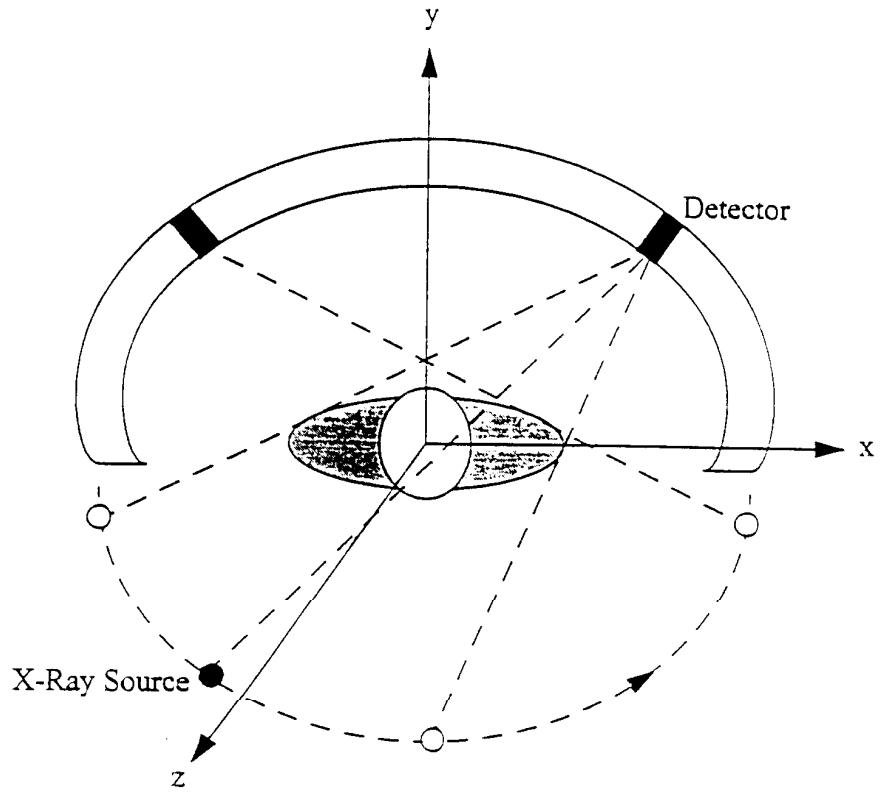


Figure 5. Electron beam CT scanner geometry. The non-circular scanning locus allows shorter x-ray source-to-detector distances, thereby increasing the signal to noise ratio.